*International Journal for Uncertainty Quantification*, 2 (2): 145–160 (2012)

# A STOCHASTIC COLLOCATION APPROACH FOR UNCERTAINTY QUANTIFICATION IN HYDRAULIC FRACTURE NUMERICAL SIMULATION

***Souleymane Zio & Fernando A. Rochinha****

*Mechanical Engineering, COPPE, Federal University of Rio de Janeiro, P.O. Box 68503, 21941-972, Rio de Janeiro, Brazil*

*Original Manuscript Submitted: 10/04/2011; Final Draft Received: 05/23/2011*

*The exploitation of oil and gas can be stimulated through hydraulic fractures (HF), which are discontinuities in the rock formation induced by the injection of high pressurized viscous fluids. Because there exists considerable variability in geologic formations, such as oil and gas reservoirs, the computational models, and, consequently, the predictions drawn from simulations, might lead to misleading conclusions, despite the use of efficient and robust numerical schemes. In order to take into account uncertainties on the numerical results due to the variability in the input data, a stochastic analysis of HF is presented here. The elasticity modulus of the rock and the confining stress are assumed to be described by random variables, and therefore, the equations governing the fracture propagation are recast as stochastic partial differential equations (SPDEs). In order to solve the resulting problem, among several alternatives available in the literature, a stochastic collocation method is adopted. The elasticity modulus probability distributions are constructed using two different approaches, both using a small amount of information. A number of numerical simulations are presented in order to illustrate the impact of the uncertainties in the data input on the fracture propagation.*

**KEY WORDS:** *hydraulic fracture, uncertainty quantification, stochastic collocation*

## 1. INTRODUCTION

Hydraulic fracture (HF) is a generic denomination for the propagation of brittle fractures in prestressed solid media resulting from the injection of pressurized viscous fluid. These tensile fractures are found in nature, as those observed on deep underground produced by pressurized magma. Many engineered processes are designed to mimic these natural phenomena. In particular, in the realm of oil and gas exploitation, HF are generated in subterranean reservoirs in order to stimulate their productivity. The fracture is initiated at a well and propagates in planar regions that are perpendicular to the direction of the minimum principal in situ confining stress. At a later stage of the stimulation treatment, proppant is added to the fracturing fluid and is then deposited in the interior of the fracture. This proppant pack is responsible for enhancing local permeability by forming a conduit to gas and oil when the treatment is finished.

Experimental tests or indirect field monitoring involving HF are expensive procedures and only provide limited information. Therefore, numerical simulation represents an appealing alternative to be used on the design and optimization of such stimulation treatments [1]. Because there exists significant variability in geologic formations such as oil and gas reservoirs [2, 3], computational simulations might lead to misleading conclusions, despite the use of reliable numerical schemes. Quantifying the impact of input uncertainties on final results of the numerical simulation has attracted considerable attention along the last few years, and various methods have been developed and applied successfully (please see [4] and reference therein).

Here, we consider the elasticity modulus of the rock formation and the confining stress uncertain parameters [2]. Under that circumstances, the original governing equations [5] are reformulated as stochastic partial differential equations (SPDEs). The interest relies not only on finding solutions expressed through first- or second-order statistical

*Correspond to Fernando A. Rochinha, E-mail: faro@mecanica.coppe.ufrj.br

2152–5080/12/$35.00  

moments, but also on quantifying the simulations output uncertainties, if one wants to increase the confidence in the predictions. Perturbation methods and sensitivity analysis [6] are employed as uncertainty quantification (UQ) methods in the realm of engineering and applied sciences, whenever uncertainties in the input data are small and the models are only slightly nonlinear. When larger uncertainties are to be considered, those methods are no longer adequate. A considerable number of methodologies for tackling this situation exploring spectral expansions of the stochastic response using polynomial chaos (PC) have been proposed recently. The use of PC for establishing a framework for UQ methods was first proposed in [7]. After that, many alternatives relying on similar ideas and concepts have been developed and, due to their effectiveness, are quite often used on complex simulation problems, replacing the traditional Monte Carlo method. Different areas have been covered ranging from fluid mechanics [8] to applications involving eigenvalue problems [9] and MEMS [10]. This was made feasible by expanding the original PC expansions, using generalized polynomial chaos (gPC) or polynomial dimensional decomposition (PDD), such that arbitrary probability distributions could be addressed [11–13]. Difficulties arising from adapting complex or commercial computational codes have stimulated the design of techniques that combine the fast convergence of polynomial expansion methods based on Galerkin projections with the nonintrusive character of sampling methods. In that context, stochastic collocation methods (SCMs) emerge as appealing alternatives. They consist of building polynomial interpolations of the stochastic solution via solving, independently, a deterministic problem for each interpolation point.

The initial ideas relying on global polynomial expansion over the stochastic dimension has shown not to be robust when the solution exhibits discontinuous dependence on the input random parameters. Convergence deterioration is observed because global polynomials are not able to resolve local discontinuities given rise to the well-known Gibbs phenomenon. Moreover, for time-dependent problems, the error of the approximation might grow substantially during long-term integration [14]. Therefore, this scenario indicates the need for more efficient and robust schemes in order to address those potential drawbacks. A deeper discussion of this topic is outside the scope of the present work, and the interested reader can find viable alternatives, based on adaptivity, to remedy those issues in [15] and [16].

Here, due to the easiness of implementation conjugated with the expected smoothness of the HF evolution with respect to the input parameters, we have adopted an SCM employing Lagrange polynomials to build the stochastic interpolation. The use of stochastic collocation was also motivated by the fact that, in the present work, we are only dealing with low-dimensional stochastic spaces, thus avoiding the so-called curse of dimensionality that poses limitations to several stochastic simulation methods [17].

The main focus of the present work is on understanding, in the context of HF simulation, the impact of the aforementioned uncertainties in the prediction of engineering quantities of interest. The stochastic computational implementation consists of building a wrapper around the deterministic code. As a deterministic solver, we use a plane-strain version of the numerical method proposed in [5]. As in any other stochastic simulation, we begin by proposing a probabilistic description of the uncertain input parameter. Two different methodologies are used. Both recognize that experimental data are scarce and difficult to obtain for HF. The first method relies on assuming a log-normal distribution; thus, only the mean and dispersion values are used to calibrate the probabilistic model. The second method employs the principle of maximum entropy [18] and is derived using the same information that is used for the obtaining the log-normal distribution.

The rest of the paper is organized as follows: In Section 2, we present the governing equations for HF evolution. In Section 3, we, briefly, introduce the collocation method used to propagate the uncertainties. In Section 4, we discuss the probabilistic modeling of the input data. In Section 5, we present a number of numerical results. Finally, we provide concluding remarks in Section 6.

## 2. HYDRAULIC FRACTURE MODELING

Hydraulic fractures naturally tend or are designed to propagate in planar regions orthogonal to the direction of the minimal confining stress. Its evolution is driven by fracturing fluid injected at high pressure, breaking the rock formation, and this fluid is partially lost because it might leak off toward the ambient rock. Therefore, the physics of the hydraulic fracture propagation involve nonlinear fluid flow, elastic deformation, and linear elastic fracture mechanics.

The model for describing HF addressed here is a one-dimensional version of the one presented in [5], as long as plane strain evolution is assumed. The resulting mathematical model, to be described below, results in a coupled

nonlinear free boundary problem involving integral and partial differential equations, which only can be solved, even in the present one-dimensional (1D) setting, with the help of numerical techniques.

The quantities of interest, to be obtained through numerical simulations, used as support to the design of HF in oil exploitation are the area covered by the fracture (often referred to as footprint), the fracture opening over this area and the fluid pressure $p_f$. The former, in the plane strain situation, is reduced to the length of the fracture 2 $\ell(t)$ and the opening field is denoted as $w(x,t)$, where $x$ and $t$ are the spatial position and the time. A schematic view of HF is depicted in Fig. 1.

Before considering, in more detail, the equations governing the problem, in the following we reproduce dimensionless quantities introduced in [5]. The use of a dimensionless form of the equations is twofold: obtaining a better conditioned numerical problem and establishing an objective basis to analyze the competition among different physical mechanisms present in hydraulic fracturing. The following change of variables is employed:

$$x = \ell_* \chi, \quad t = t_* \tau, \quad \ell(t) = \ell_* \gamma(\tau), \quad p = p_* \Pi, \quad \mathrm{w} = \mathrm{w}_* \Omega, \quad \sigma_0 = p_* \Sigma_0 \phi(\chi) \tag{1}$$

where $\ell_*$, $t_*$, $p_*$, and $w_*$ represent characteristic length, time, pressure, and openning. The quantities $\chi$, $\tau$, $\gamma$, $\Pi$, and $\Omega$ represent the dimensionless spatial coordinate, the dimensionless time, fracture front locations in dimensionless coordinates, the dimensionless pressure, and the dimensionless fracture opening, respectively. Moreover, $\sigma_0$ is the geological confining stress, with spatial distribution $\phi(\chi)$ and nondimensional magnitude given by $\Sigma_0$. The use of this change of variables yields on the following dimensionless quantities:

$$g_e = \frac{E' \mathrm{w}_*}{p_* \ell *}, \quad g_m = \frac{\mathrm{w}_*^2 p_* t_*}{\mu' \ell_*^2}, \quad g_v = \frac{Q_0 t_*}{\mathrm{w}_* \ell_*}, \quad g_c = \frac{C' t_*^{1/2}}{\mathrm{w}_*}, \quad g_k = \frac{K' \ell_*^{1/2}}{E' \mathrm{w}_*} \tag{2}$$

where $E' = E/(1-\nu^2)$, $E$ and $\nu$ are the rock elasticity modulus and Poisson's ratio; $\mu' = 12\mu$, where $\mu$ is the dynamic fluid viscosity; $Q_0$ is the volumetric injection rate per unit length in the out-of-plane direction; $C' = 2C_L$, where $C_L$ is Carter's leak-off coefficient; and $K' = 4(2/\pi)^{1/2} K_{IC}$ is the modified stress intensity factor.

Although there is a number of analytical and numerical models of HF with varying complexity [1], we choose a model comprising a hydraulic fracture propagating in a state of plane strain (an extended version of the so-called also KGD model) in order to assess the impact of input data uncertainties. This model is employed here as, although its relative simplicity, it encompasses a number of key propagation modes and physical effects, such as spatially varying and even discontinuous confining stress fields and Carter leak-off, while maintaining a relatively modest computational cost. Hydraulic fracturing is a complicated process to model, as it involves the coupling of at least three distinct

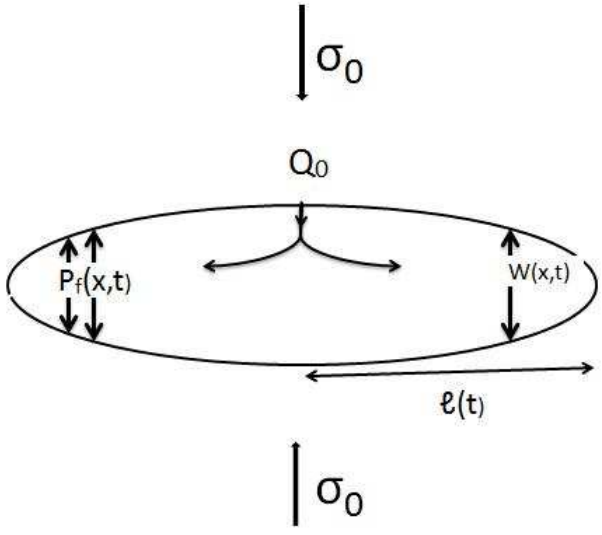


**FIG. 1:** Schematic view of a hydraulic fracture.

physical processes: the mechanical deformation induced by the fluid pressure on the surrounding rock, the flow of fluid within the fracture, and the fracture propagation. The rock deformation is governed by an elasticity equation, relating the fluid pressure and the deformation of the surrounding media. The fluid flow, due to the particular characteristics of the flow along the crack, is modeled by the Reynold's lubrication theory. Moreover, boundary conditions describe the crack propagation conditions. The criterion for fracture propagation is given by the conventional energy-release rate approach of linear elastic fracture mechanics theory (LEFM). The equations are briefly presented in the dimensionless form, as follows:

### 2.1 Elasticity Equation

$$\Pi = \Pi_f(\chi,\tau,\omega) - \Sigma_0(\omega)\Phi(\chi,\omega) = -\frac{g_e}{4\pi}\int_{-\gamma(\tau,\omega)}^{\gamma(\tau,\omega)} \frac{\Omega(\chi',\tau,\omega)}{(\chi-\chi')^2}\,d\chi' \tag{3}$$

where $\Pi$ stands for the net pressure.

### 2.2 Fluid Flow Equation

$$\begin{aligned}\frac{\partial\Omega(\chi,\tau,\omega)}{\partial\tau} + g_c\frac{H[\tau-\tau_0(\chi)]}{\sqrt{[\tau-\tau_0(\chi)]}} &= \frac{1}{g_m}\frac{\partial}{\partial\chi}\left[\Omega(\chi,\tau,\omega)^3\frac{\partial\Pi_f(\chi,\tau,\omega)}{\partial\chi}\right] + g_v\Psi(\tau)\delta_0(\chi) \\ &- \gamma(\tau,\omega) < \chi < \gamma(\tau,\omega)\end{aligned} \tag{4}$$

where $H$ is the Heaviside function and its argument $\tau_0$, not known a priori, denotes the time that the point $\chi$ within the fracture was first exposed to the fluid. Moreover, $\Psi(\tau)$ is the dimensionless injection rate and the Dirac delta $\delta_0(\chi)$ defines the position of the injection well.

Besides the space and time coordinates $\chi$ and $\tau$, we introduce $\omega$, the third argument for the fields above, in order to represent the random dimension to be introduced in detail later and needed for describing uncertainties. Formally, the solutions to be obtained by solving the mathematical problem resulting from the modeling are sought in functional spaces resulting from a tensor product between canonical space-time spaces and a complete probability space $(\Gamma,\mathcal{F},P)$. $\Gamma$ stands for the space of outcomes, $\mathcal{F}$ is the corresponding σ-algebra (set of all subsets often referred to as events), and $P:\mathcal{F}\to[0,1]$ is the probability measure.

### 2.3 Boundary and Propagation Conditions

A zero flux boundary condition is imposed on the fracture boundary $\chi=\gamma(\tau,\omega) \quad \chi=-\gamma(\tau,\omega)$

$$\lim_{\xi\to 0}\Omega^3\frac{\partial\Pi_f}{\partial\xi} = 0 \tag{5}$$

where $\xi=\gamma-\chi$ is a local coordinate representing the distance from a fracture interior point to the fracture tip. The evolution of the moving boundary is governed by the classical condition derived from (LFEM)

$$\lim_{\xi\to 0}\frac{\Omega}{\xi^{1/2}} = g_k \tag{6}$$

where $g_k$ is the dimensionless rock toughness defined in Eq. (2).

The asymptotic square-root condition (6), only prevails in a tiny region of the domain, which might not be captured at the computational length scale. Moreover, immediately behind, in a so-called near-tip region, another asymptotic trend develops within a layer, which can be tracked by means of reasonable spatial discretization schemes. This last asymptotic behavior strongly influences the dynamics of the whole system. Indeed, HF evolution results from the competition of two physical process involving dissipation and fluid balance. Here, we will not consider leak off ($g_c = 0$) and, therefore, all fluid injected along the treatment is stored within the fracture. Thus, only dissipation

mechanisms will determine the dominant characteristics of the evolution. Dissipation is due to the viscosity of the fluid flowing through the fracture cavity and to energy needed to fracture the rock. Typically, the HF starts in the so-called viscous-dominated regime ($g_c$ = $g_k$ = 0) in which the main part of energy is lost to the flow. Along the fracture evolution, the energy loss for breaking the rock tends to increase. Nevertheless, the viscous dominate regime endures for a period, which goes way beyond the treatment time. That justifies to consider only the dissipation associate to the fluid flow. More details about the multiphysics and multiscale behavior of HF can be found in [5].

Assuming the viscous dominated regime, the fracture tip asymptotic behavior of the fracture is considered to follow the following condition below [5], which is weakly enforced within the deterministic solver and plays a crucial role in the determination of the fracture front.

$$\mathrm{w} \sim 2\ \ 3^{7/6}\,(\mu/E')^{1/3}\,V^{1/3}(\xi\ell_*)^{2/3} \tag{7}$$

The above asymptotic is presented in a dimensional form to establish the connection of the fracture opening $w$ in the near-tip region and the elasticity modulus, which will be considered an uncertain input parameter. In Eq. (7), $V$ stands for the fracture propagation velocity.

## 3. STOCHASTIC FORMULATION AND UNCERTAINTY QUANTIFICATION

In order to obtain reliable predictions from numerical simulations, two key ingredients are in need: a robust numerical solver and a method to propagate unavoidable uncertainty present in the input data. Here, in order to understand better the impact of such uncertainties on the output of the simulations, we employ the implicit level-set algorithm (ILSA) developed in [5], which has been exhaustively assessed and proved to be efficient and stable as a deterministic solver. Because it requires a dedicated computational code with many particular features, a nonintrusive uncertain propagation scheme is more convenient. The uncertainties are characterized through random variables, implying that the sought solution of the hydraulic fracture evolution problem consists of stochastic fields representing the opening of the fracture $\Omega[\chi,\tau,\boldsymbol{\theta}(\omega)]$, its length $\ell[\tau,\boldsymbol{\theta}(\omega)]$, and the net pressure field $\Pi[\chi,\tau,\boldsymbol{\theta}(\omega)]$ belonging to the functional spaces mentioned previously. $\boldsymbol{\theta}(\omega)$ is a finite $d$-dimensional vector with identically distributed continuous random variables $\theta_k$ as components defined over the stochastic support $\Gamma_S \subset \Gamma$. Admitting $\theta_k$ ($k = 1,...,d$) mutually independent with PDFs $\rho_k(\theta_k)$, the joint PDF is written as $\rho(\boldsymbol{\theta}) = \prod_{k=1}^{d} \rho_k(\theta_k)$.

By characterizing the uncertainty through random variables, we ended up with a stochastic time-evolution problem defined over a $(d+1)$-dimensional space. As a stochastic solver for numerically solving that problem, we opted for using the nonintrusive SCM [19], which has been proved more efficient than traditional sampling methods like Monte Carlo, often employed in engineering applications. At this point, it is worth mentioning that the choice of a SCM relies on the expectation of having enough smoothness of the response with respect to the uncertain input data and, also, on dealing with stochastic low-dimensional inputs. The presence of discontinuities entails the need for more efficient and robust numerical schemes like those mentioned in the Section 1.

We will not present ILSA used to solve the deterministic nonlinear free-boundary problem because it can be inserted as a blackbox in the computational framework provided by stochastic collocation. The interested reader can find all details about this deterministic solver in [5], but it is worth remarking that this key ingredient relies on enforcing, as a boundary condition for the crack evolution, the relation (7) at the elements of the computational grid containing the fracture tip. This asymptotic condition involves the uncertain elasticity modulus.

The basic idea of the collocation approach is to approximate the solution by a polynomial interpolation defined over a multidimensional random space associate to the uncertainties. This polynomial interpolation is built using the problem solution computed at a set of $M$ points in the stochastic space $\left[\Theta^j_{M(j)} = \{\boldsymbol{\theta}_i\}_{i=1}^{M(j)}\right]$. At each one of those points, we solve the fracture evolution problem in order to obtain the fields variables $\Omega^j(\chi,\tau,\boldsymbol{\theta}^j_i)$, $\Pi^j(\chi,\tau,\boldsymbol{\theta}^j_i)$, and $l^j(\chi,\tau,\boldsymbol{\theta}^j_i)$. The integer index $j$ denotes the level of the interpolation (number of employed interpolation points) and, consequently, is related to its accuracy. Therefore, the interpolated stochastic fields for a specified level [fixed number of interpolation points: $M(j)$] are built as follows:

$$(\widehat{\Omega}^j, \widehat{\Pi_f}^j, \widehat{\ell}^j) = \sum_{k=1}^{M} \left[\Omega(\xi,\tau,\boldsymbol{\theta}^j_k), \Pi_f(\xi,\tau,\boldsymbol{\theta}^j_k), \ell(\xi,\tau,\boldsymbol{\theta}^j_k)\right] L^j_k(\boldsymbol{\theta}) \tag{8}$$

where $L_k$ are chosen as multivariate Lagrange polynomials. There are a number of different possibilities for choosing the set of the collocation points. Typically, one selects a distribution of points in one dimension and obtains the grid for the multidimensional domain through tensor products of this (1D) set of points. In order to keep the number of deterministic evaluations minimal, trying to avoid the so-called curse of dimensionality, sparse grid techniques [20] are often employed. We adopted, in one dimension, the Clenshaw-Curtis points, the nonequidistant extreme of Chebyshev polynomials [16]. These 1D points combined with the Smolyak quadrature allows for a nested implementation $\left[\Theta^{j+1}_{M(j+1)} \supseteq \Theta^{j}_{M(j)}\right]$, such that hierarchical interpolations can be easily obtained. Thus, aiming at obtaining a more accurate approximation, a new level $j+1$, corresponding to an increase on the number of interpolation points, might be employed. The $d$-dimensional grid is built with the help of sparse grid strategies and we only need to compute the deterministic solution associate to the new points added to the grid. Ad hoc convergence criteria can be used in order to select the final approximation level $j$.

The statistics of the solution, represented by $m$th moments of the random response (8), can be estimated in a straightforward way by either performing the corresponding integrals or by sampling the distribution $\rho(\boldsymbol{\theta})$. The first option leads to the computation of integrals of products between the joint PDF and the interpolation polynomials over the stochastic support, which can be calculated beforehand. Sampling appears as an appealing way to obtain the statistics, if this calculus become tedious due to high dimensionality. In this case, depending on the PDF, costless automatic generator of random variables can be used, as it is the case for standard and uniform variables. Typically, the sought statistics are low moments as mean values or variance. Even reasonable approximations of the PDF can be computed by employing enough collocation points and samplings. It is worth mentioning that obtaining those response statistics is carried out by a postprocessing of the computed deterministic solutions, not representing a significant increase on the computational costs, even when more sophisticated numerical schemes are needed for sampling. It is also interesting to remark that the analytical representation of the solution (8) allows one to create an explicit connection among input and output uncertainties regarding a sensitivity analysis.

## 4. MODELING INPUT UNCERTAINTY

The SCM, briefly described in the Section 3, is capable of propagating uncertainties in the input data that should be characterized before the computations. The present section is devoted to discussing alternatives, within an engineering perspective of HF, for modeling those uncertainties. The model parameters are organized into dimensionless quantities (2), but we address the set of parameters present in the governing equations before scaling because their physical meanings help on characterizing the potential uncertainties. Besides, we eliminate from this set the leak-off ($C'$) and elastic toughness ($K'$) parameters because we assume that fracture evolves in the viscosity-storage regime ($g_c = 0$ and $g_k = 0$). Therefore, the remaining parameters are the elastic modulus ($E'$), the fluid viscosity ($\mu'$), and the rock confining stress ($\sigma_c$).

The viscosity of the injected fluid can be assessed through accurate laboratory tests. Therefore, we do not expect the same amount of uncertainty in this parameter when compared to the other two. Indeed, the difficulties arising from the rock being located underneath at large distances from the free surface lead to a scenario of scarce data and indirect measurements or test laboratories carried out on different ambient conditions. Those factors lead to imprecise descriptions of the input parameters present on the HF modeling [2, 3, 21].

Because of the strong nonlinear character of the HF model, we decided to isolate effects and emphasize the impact of the elasticity modulus's uncertainties on the problem solution. Because the hydraulic fracture is designed such to remain within a layer of the rock, this modulus is considered spatially homogenous along the fracture surroundings. Its variability is attributed only to the factors already discussed, and it is modeled by means of a random variable.

Considering that the most reliable available data consists of a small number of samples such that mean, variance, and the dispersion interval can be estimated, we built two different probabilistic models in order to describe the random elasticity modulus. The first relies on assuming a log-normal probability distribution, which enforces that any realization of the random variable is positive. The modulus is conveniently rewritten as $\widetilde{E'}=(\overline{E'}/1+\kappa)(1+\kappa\varepsilon)$, where $\kappa$ regulates the variance and $\varepsilon$ is a random variable with a Log-normal distribution with mean and variance

equal to 1. The parameter $\kappa$ will be explored later to analyze the sensitivity of the response with respect to the level of uncertainty in the input data.

The second approach borrows its main ideas from [22, 23], where the maximum entropy principle (MaxEnt) [24] is explored such that the construction of a stochastic model for $\widetilde{E'}$ is cast as a constrained optimization problem. Entropy is considered as a measure of information quantification [25] and expressed through the following function of the random variable PDF:

$$\Upsilon(p_{\boldsymbol{\theta}}) = -\int_{\Gamma_S} p_{\boldsymbol{\theta}}(\theta)\,\log[p_{\boldsymbol{\theta}}(\theta)]\,d\theta \tag{9}$$

We seek for a probability distribution that maximizes (9) and satisfies the constraints associated to the available information. We parametrize the elasticity modulus as $\widetilde{E'} = \overline{E'}(1+\epsilon)$, with $\epsilon$ a random variable with PDF computed by solving this optimization problem constrained by the following three conditions:

$$\int_{\Gamma_S} g_i(\theta)\,p_{\boldsymbol{\theta}}(\theta)\,dx = E[g_i(\boldsymbol{\theta})] = a_i, \quad i = 0,1,2 \tag{10}$$

where $g_0(x) = 1$, $g_1(x) = x$, and $g_2(x) = x^2$. Therefore, the first condition enforces normalization of the PDF, the second and third correspond to setting a value for mean and variance. In order to establish a meaningful comparison between the two different stochastic models for the elasticity modulus, $a_1$ and $a_2$ are taken, respectively, equal to $0$ and $0.1$. Moreover, the support $\Gamma_S$ was designed to contain $96\%$ of the samples from the log-normal distribution corresponding to the first model ($0.6 \leq \widetilde{E} \leq 1.4$). The constrained optimization problem was turned into an unconstrained one by using Lagrange multipliers and solved through a Newton-Raphson numerical scheme. The solution is finally given by the following PDF:

$$p_\epsilon = \mathcal{I}_{[-0.6,0.6]}\; e^{(0.022-1.863\epsilon^2)} \tag{11}$$

where $\mathcal{I}$ and $e$ stand, respectively, for the indicator and exponential functions. We generated samples of the resulting PDF by using a Markov Chain Monte Carlo method [26, 27]. The PDFs for both models are presented in the form of histograms in Figs. 2 and 3.

Both models yield random elasticity modula sharing the same mean ($\overline{E'}$) and variance, as long as $\kappa$ is equal to $0.1$. This value for $\kappa$ also insures that the samples drawn from $\widetilde{E'}$ fit into the range of variability observed in the field [2, 21].

## 5. NUMERICAL RESULTS

In the present section, we employ the hydraulic fracture probabilistic model introduced earlier to quantify the impact of uncertainties on the fracture evolution prediction. More specifically, we consider the effect of uncertainties in the elasticity modulus and the confining stress on fracture opening, well pressure, and fracture footprint. Before analyzing

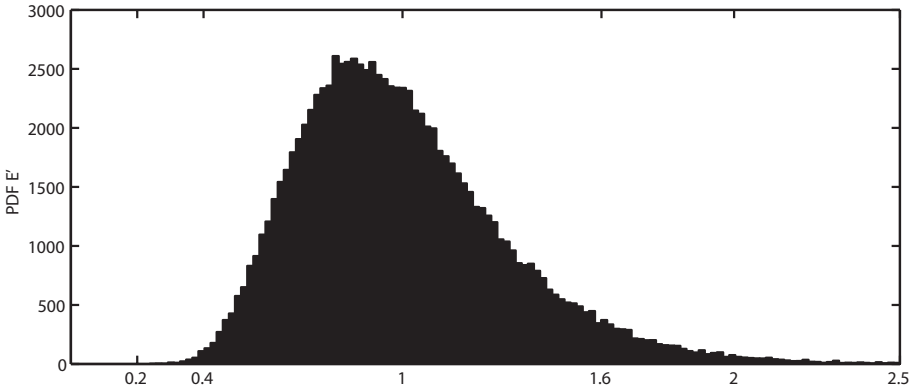


**FIG. 2:** Log-normal distribution of the elasticity modulus.

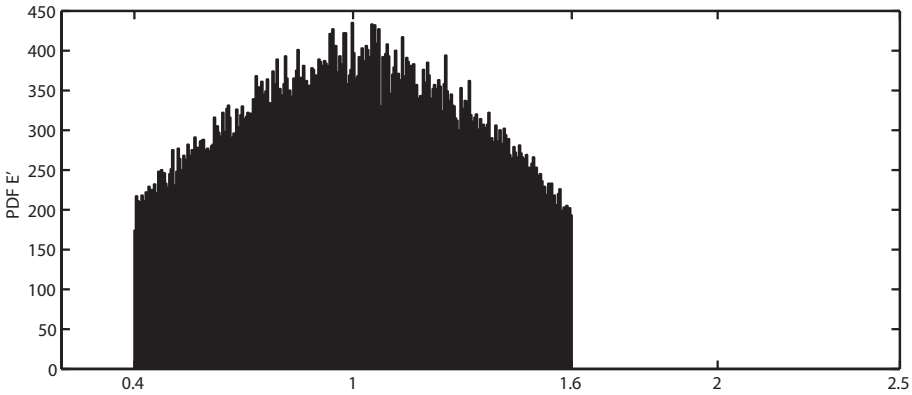


**FIG. 3:** Distribution probability density function of the elasticity modulus computed with MaxEnt.

the uncertainty propagation, we also present a brief summary of the SCM's computational performance by comparing its results to Monte Carlo simulations.

### 5.1 Computational Performance

We consider, for an initial assessment of the computational performance of SCM when applied to the current stochastic model, a hydraulic fracture propagating in the viscosity-storage dominating regime under a homogeneous confining stress and a constant volumetric flow rate $Q_0$. For that situation, there is a semianalytical solution [28] for the deterministic problem, which helps on optimizing the spatial and time discretization schemes ($\Delta\chi = 2$, $\Delta\tau = 10$). By doing that, we intend to isolate the effects of the uncertainty in the parameter model on the responses. In those numerical experiments, we consider as the unique uncertain input the elasticity modulus with a log-normal distribution with unity mean and standard deviation equal to $0.1$. We use, as figure of merit, the opening field $\Omega$ at specified times, namely, $\tau = 53$, $\tau = 105$, and $\tau = 158$, which are representative of the trends and behavior observed along the whole simulation.

In order to assess the convergence of the collocation method with respect to the stochastic dimension, we employ a reference solution obtained by Monte Carlo method replacing an exact solution, which is not available. This reference solution was computed using $3500$ samples of the random input, which was enough for achieving an accurate approximation for mean and variance of the output. Convergence of both methods were then studied through the error on the mean values of the response for the above-cited fixed times. The error measure is given by the spatial averaged norm of the difference between computed mean values and those of the reference solution normalized by the absolute value of the last one. At that point, it is worth mentioning that the computational cost associated with each method is legislated by the number of calls to the deterministic solver, which, for Monte Carlo, is the number of sampling points, whereas, for collocation, it corresponds to the number of interpolation nodes on the stochastic support space. Indeed, as stated before, the statistics of collocation solution were computed by sampling the approximated solution (8), which adds almost nothing to the final computational cost.

Convergence studies are depicted in Figs. 4 and 5, and clearly, for the present computations, SCM outperforms Monte Carlo. Monte Carlo requires almost 3000 sampling points for attaining an error equal to $2 \times 10^{-3}$. Collocation achieved the same error at interpolation level 3, which, for the selected grid of points, demands the computation to be performed only in nine interpolation nodes. Although not presented here, the convergence behavior for the variance follows a similar pattern.

In order to stress the accuracy of the computed solutions using SCM, we present, in Fig. 6, a comparison among the reference Monte Carlo solution for the fracture opening mean $\overline{\Omega}(\chi, \tau = 158)$ and the approximations obtained with SCM for levels 1–4 of interpolation. In this figure, we label the different levels of interpolation by their corresponding number of interpolation nodes, which makes easier an assessment of the required computational effort.

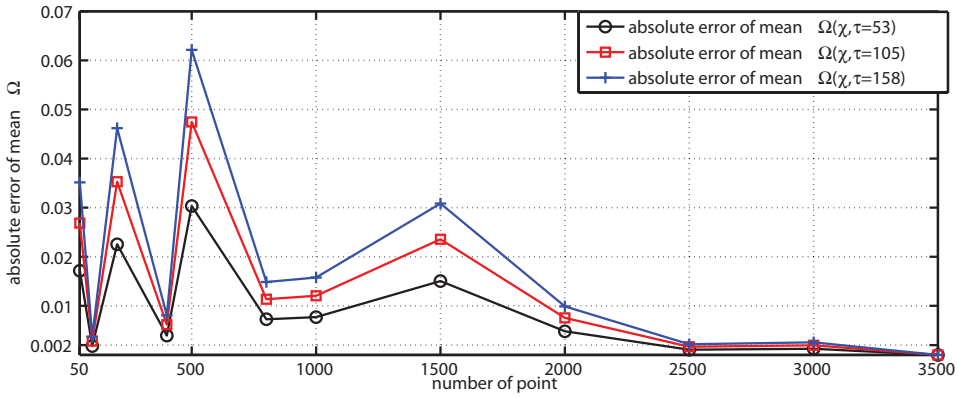


**FIG. 4:** Convergence of Monte Carlo simulation.

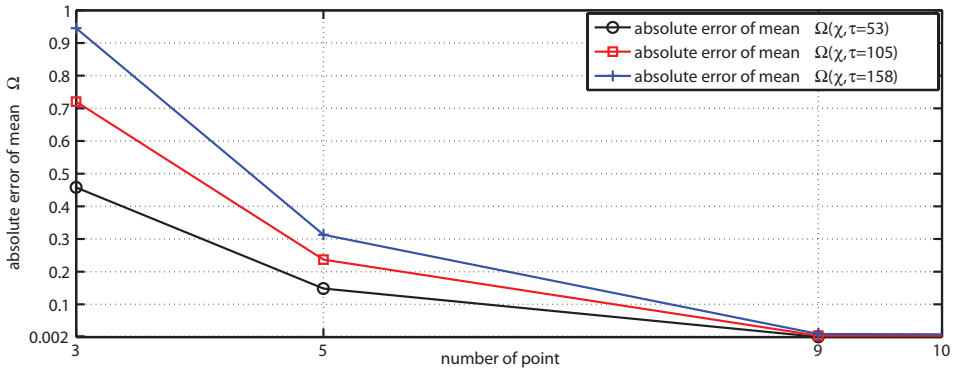


**FIG. 5:** Convergence of stochastic collocation method.

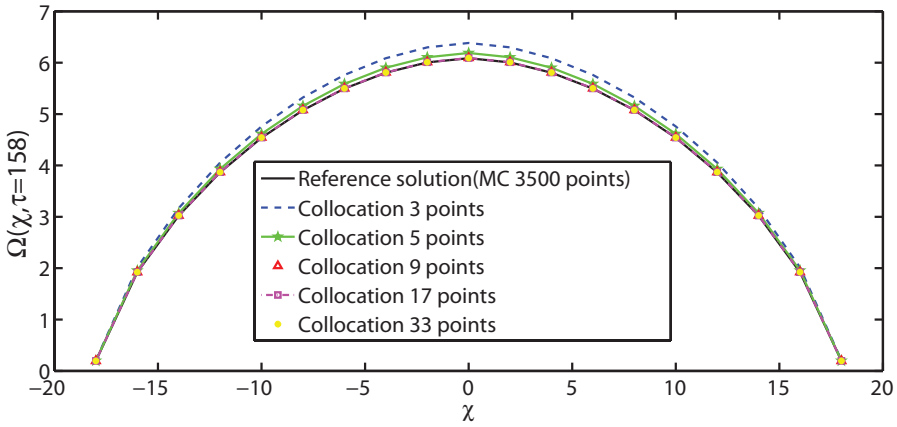


**FIG. 6:** Stochastic collocation computed fracture opening fields for different interpolation levels compared to the Monte Carlo reference solution.

Often, high-order statistics are required; thus, we also investigated the convergence of the PDF of the fracture opening at the injection point at $\tau = 158$. Figure 7 depicts the PDFs obtained by sampling the solution (8) for different levels ($j = 1, ..., 4$) of interpolation. Again, the interpolation levels were labeled with the total number of corresponding grid points. In Fig. 7, we postprocessed the interpolated solution using 5000 sampling points.

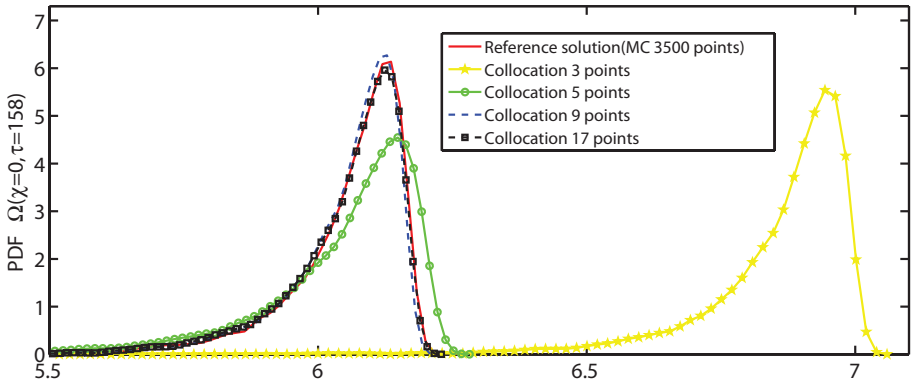


**FIG. 7:** Stochastic collocation computed PDFs for different interpolation levels compared to the Monte Carlo reference solution.

### 5.2 Hydraulic Fracture Uncertainty Quantification

Now, we go deeper on understanding how the uncertainty on the elasticity modulus propagates along the fracture evolution. The same conditions applied to the previous example are considered here, but a different study is carried out aiming at emphasizing UQ aspects of the problem. We also use the same discretization parameters for spatial and time domain. The stochastic components of the hydraulic fracture evolution are resolved employing SCM with interpolation level 4. Again, unless stated otherwise, all results were obtained using a log-normal distribution for the elasticity modulus.

In Fig 8, we present the mean fracture fracture opening at injection times $\tau = 53$, $\tau = 105$ and $\tau = 159$ with error bars twice the size of the standard deviation. We observe that uncertainties on the fracture opening increases with time and are larger at the region near the well.

Figure 9 depicts the sensitivity of the output uncertainty with respect to the degree of variability of the input data. In Fig. 10, we plot the PDFs of fracture opening at the injection well $\Omega(\chi = 0, \tau = 411)$, which seems to be the most critical within the fracture domain, as previously observed. We analyze the responses for three different values of $\kappa$, which, as stated before, modulates the standard deviation of the input data. The patterns of uncertainty are remarkably different, reflecting the nonlinear relationship between input and output data.

We now observe, through Fig. 10, that a priori inferences about uncertainty propagation based on the input are not feasible. In that figure, we depict the computed PDF of fracture opening at the well at injection time $\tau = 411$. In Fig. 10, we present an entirely different PDF corresponding to a log-normal distribution, the same type of probability

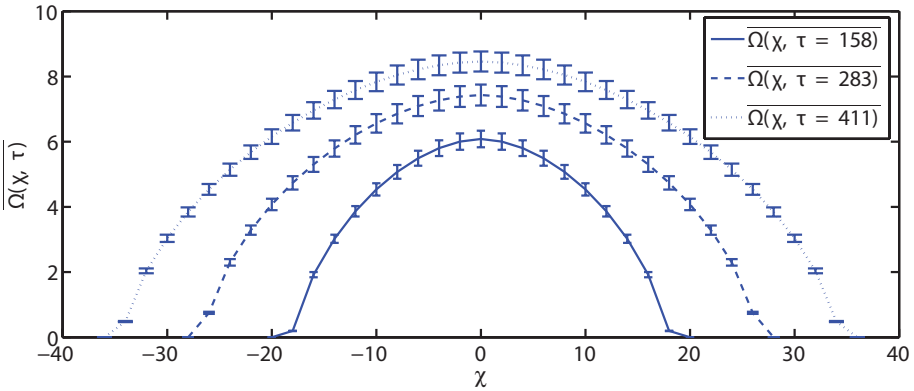


**FIG. 8:** Effect of the input uncertainty on the fracture opening field for different injection times.

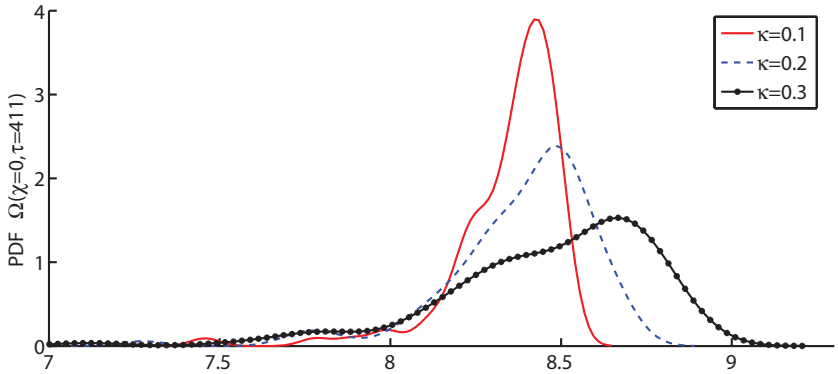


**FIG. 9:** $\Omega(\chi = 0, \tau = 411)$ uncertainty response for different standard deviations of the input data.

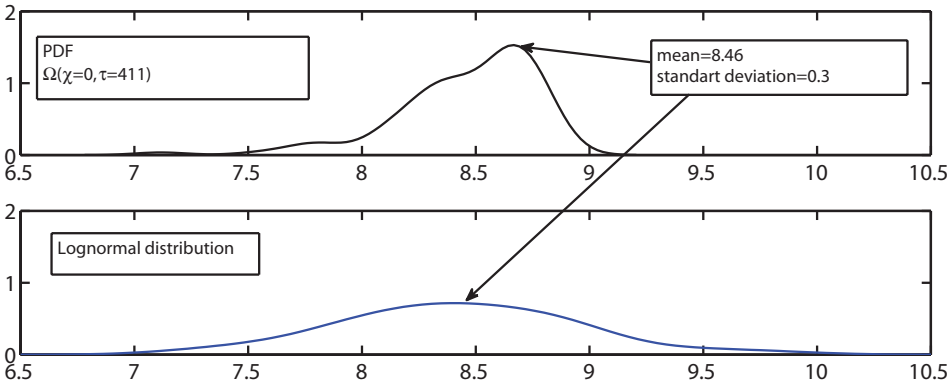


**FIG. 10:** Computed PDF of the fracture opening at the injection well $[\Omega(\chi = 0, \tau = 411)]$.

law of the input, with the same expected value and variance of the computed solution. The output (top figure) departs significantly from log-normality.

Now, the sensitivity with respect to the input uncertainty modeling is assessed. We analyze the HF response using the two different stochastic models developed previously in Section 4. The evolution of the HF is summarized through Figs. 11 and 12. The computed results with the two input models are quite different. Uncertainties on $\Omega(\chi = 0, \tau)$

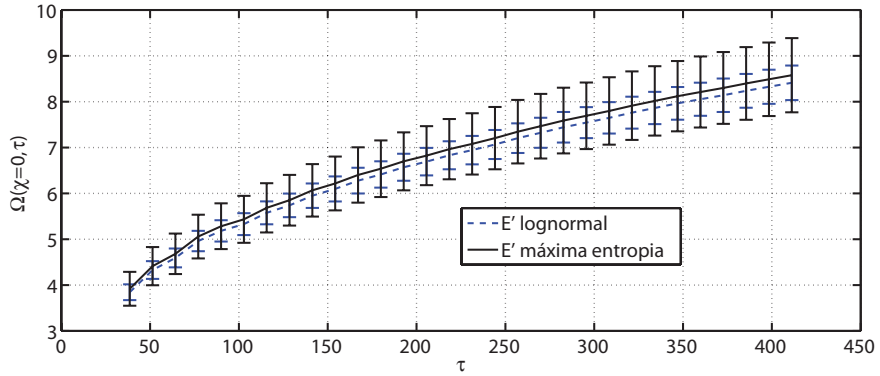


**FIG. 11:** Time evolutions of the fracture opening at the injection well $[\Omega(\chi = 0, \tau)]$ computed with the two different input models.

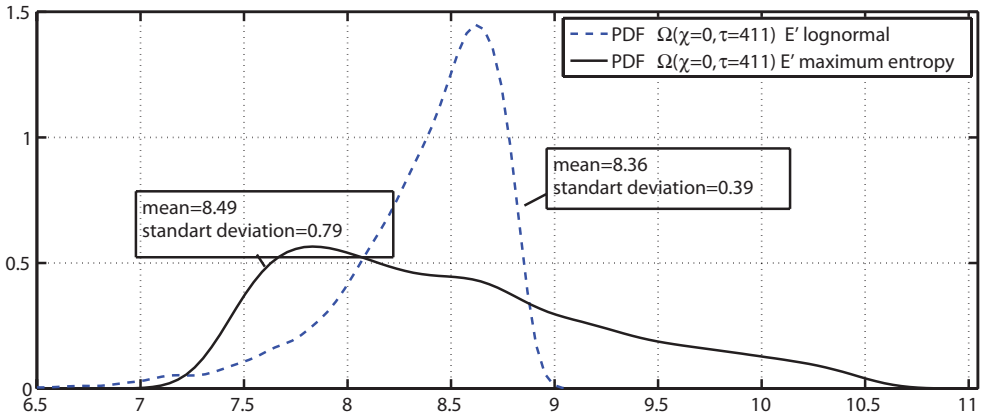


**FIG. 12:** PDF of the fracture opening at the injection well $\Omega(\chi = 0, \tau = 411)$ computed with the two different input models.

tend to be larger when we employ the elasticity modulus model built based on the MaxEnt principle. These differences are made more remarkable by comparing the two PDFs of $\Omega(\chi = 0, \tau = 411)$, as depicted in Fig. 12.

Numerical predictive models provide a basis for enabling monitoring processes through inverse formulations. Particularly, hydraulic fracture evolution monitoring is essential and a complex task, inasmuch as it occurs underneath and only can be tracked by means of indirect measurements using microseismic signals or tiltimeters. This last technology provides the deformation of the rock at specific points where the sensors are placed, usually quite a distance away from the fracture. Recently, an inverse formulation combining extended Kalman filter, tiltimeters, and the forward model discussed above was proposed in [29]. Here, we carry out a prior assessment of the sensitivity of this inverse formulation to uncertainties on the forward model by simulating the tiltimeters measurements. The variability in the response is presented on Fig 13, where a confidence interval is plotted around the expected value of the sensor signal along the time.

We now illustrate the impact on the fracture evolution when uncertainties on the stress confining are also considered. In the present modeling, as stated in (1), the confining stress $\sigma_0$ is defined by its magnitude $\Sigma_0$ and spatial distribution $\phi(\chi)$. In the previous simulations, we have considered that both were certain, known, and spatially uniform. In the next results to be presented, both magnitude and spatial distribution will be taken as uncertain. The confining stress field will be supposed to change linearly around the well position $[\phi(\chi) = \alpha_1\chi]$ with angular orientation (the angular coefficient of linear distribution $\alpha_1$) described by a random variable. Indeed, both magnitude and

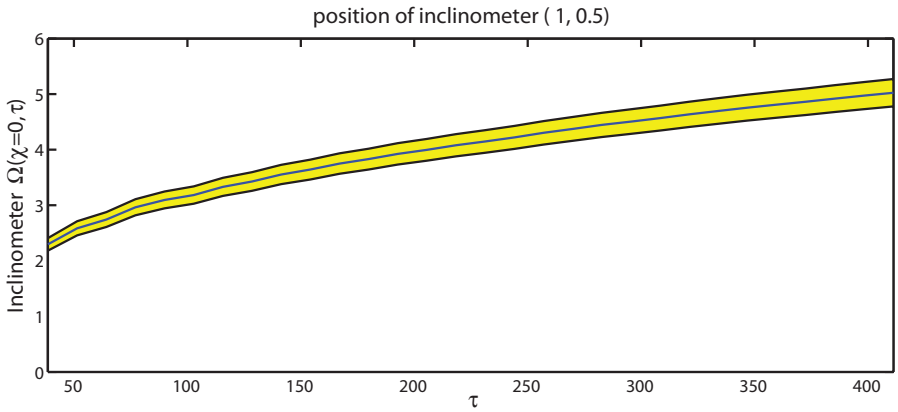


**FIG. 13:** Deformation evolution monitored with a tiltimeter: average value and confidence interval.

orientation are modeled as random variables and assumed mutually independent with log-normal probability law, and their variability are consistent with observed field data [2, 30].

Therefore, we are dealing with a three-dimensional stochastic support space because the Elasticity Modulus is still considered uncertain. As mentioned earlier a Smolyak algorithm was used to generate a sparse grid for the interpolation points. After a number of initial convergence tests consisting on refining the interpolation level and comparing the computed results, we fixed, for all results below, the level on 4 (corresponding to 177 interpolation nodes in the 3D grid).

In order to evaluate the output sensitivity with respect to input uncertainty, we plot, in all figures appearing in the sequence, both the results not considering and taking into account the added uncertainty associated to the confining stress field. The results obtained from the different sets of uncertain parameters are labeled as 1D and 3D in reference to the dimensionality of the corresponding stochastic space.

First, we remark the significant difference between the pressure responses at the injection well. The mean pressure evolution is presented in Fig. 14. The comparison between the two curves reveals that not only the mean values achieve different values. Also, the uncertainty on the predicted pressure is much more accentuated in the 3D case. That indicates a strong dependence of the pressure injection on the confining stress.

Also, remarkable differences are found when the PDFs of fracture opening at the injection well are compared, as depicted in Figs. 15 and 16. These two figures help us understand the structure of the uncertain solution and its dependence on the input parameters. They present the evolution of uncertainty on the fracture opening along the time. It is noticeable that assuming different hypothesis about the input data leads to significant different predictions.

A nonuniform confining stress engenders a spatially heterogeneous load applied to the fracture. That allows for a non symmetric evolution of the fracture, which is contemplated, thus, by the model containing the uncertain confining

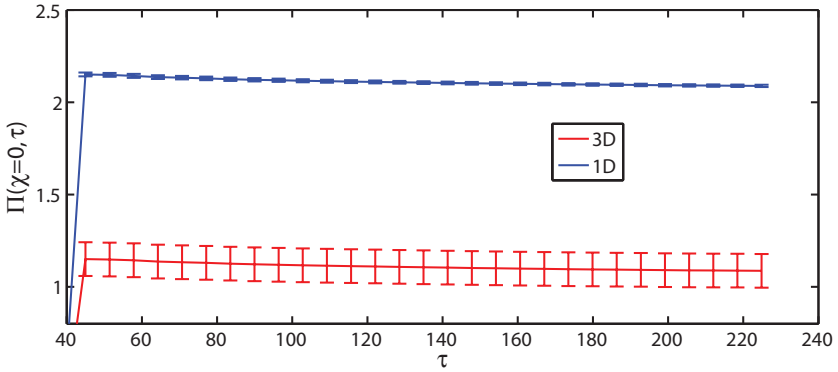


**FIG. 14:** Mean pressure evolution at the injection well.

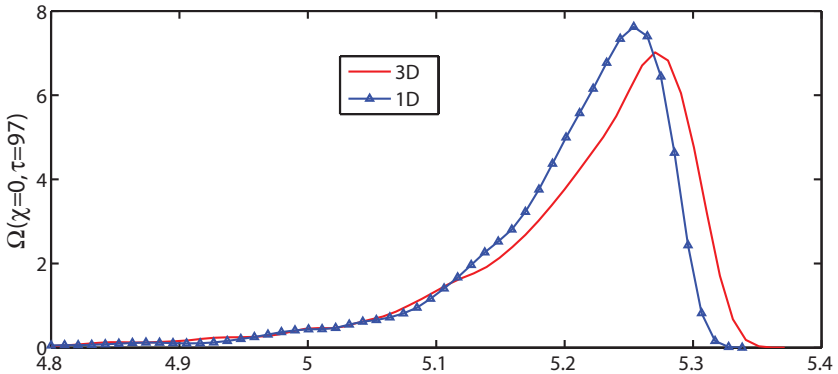


**FIG. 15:** PDFs of fracture opening at the injection well at $\tau = 97$.

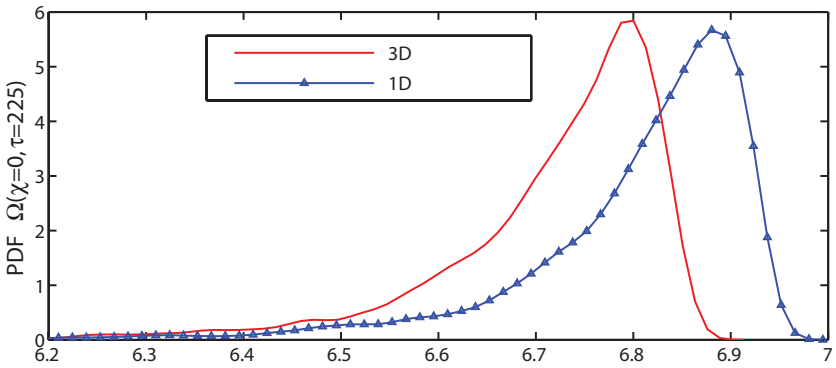


**FIG. 16:** PDFs of fracture opening at the injection well at $\tau = 225$.

stress (3D model). Figure 17 depicts the evolution of the mean of the fracture half length along with variability for both models. There are two curves for the 3D model due to the nonsymmetric evolution mentioned before.

## 6. FINAL COMMENTS

The present work investigates hydraulic fracture computational simulation in the presence of uncertainties on the input parameters. We employ a stochastic collocation framework to quantify the effect of such uncertain parameters, here limited to the elasticity modulus and the geological confining stress, on engineering quantities of interest, such as fracture extension and opening. The stochastic simulations require the modeling of the uncertainty on the inputs through random variables and propagates those uncertainties using a polynomial interpolation defined over the random domain. The modeling of the parameters, based on limited information, has followed two paths, leading to two different input models. The resulting predictions have shown to be quite sensitive to the choice of the stochastic input model.

The stochastic collocation framework leads to the computation of a number of independent deterministic problems, similarly to classical Monte Carlo simulation. Indeed, the difference to Monte Carlo relies on potential savings of computational costs. A number of numerical simulation demonstrate that, for the present application, the collocation method outperforms Monte Carlo. It is again adequate to emphasize that this good performance of SCM is related to the smoothness of the HF response and to the low dimensionality of the analysis performed in the present work.

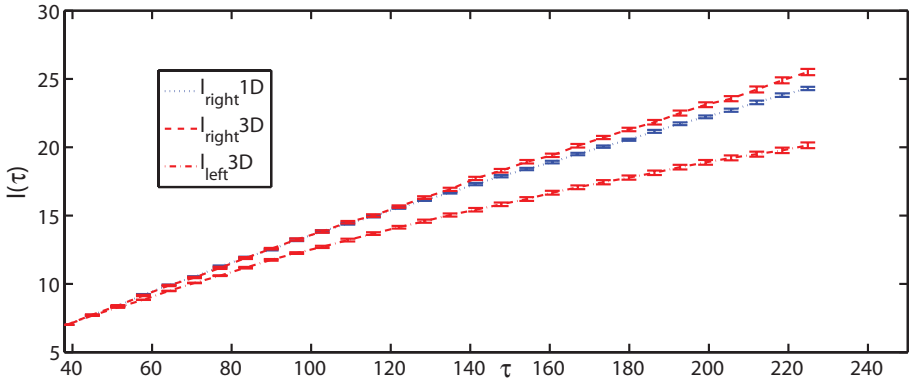


**FIG. 17:** Nonsymmetric fracture length evolution.

## ACKNOWLEDGMENTS

We express our gratitude to Prof. A. Peirce for insightful discussions on numerical modeling of hydraulic fracture.

## REFERENCES

1. Adachi, J., Siebrits, E., Peirce, A., and Desroches, J., Computer simulation of hydraulic fractures, *Int. J. Rock Mech. Mining Sci.*, 44(5):739–757, 2007.
2. Ask, D., Evaluation of measurement-related uncertainties in the analysis of overcoring rock stress from Äspö HRL, Sweden: A case study, *Rock Mech. Mining Sci.*, 40:1173–1187, 2003.
3. Miranda, T., Correia, A. G., and Sousa, L. R., Bayesian methodology for updating geomechanical parameters and uncertainty quantification, *Int. J. Rock Mech. Mining Sci.*, 46:1144–1153, 2009.
4. Ma, X. and Zabaras, N., A stochastic mixed finite element heterogeneous multiscale method for flow in porous media, *J. Comput. Phys.*, 230:4696–4722, 2011.
5. Peirce, A. and Detournay, E., An implicit level set method for modeling hydraulically driven fractures, *Comput. Methods Appl. Mech. Eng.*, 197(33-40):2858–2885, 2008.
6. Kleiber, M. and Hien, T., *The Stochastic Finite Element Method: Basic Perturbation Technique And Computer Implementation*, Wiley, Hoboken, NJ, 1992.
7. Ghanem, R. and Spanos, P. D., *Stochastic Finite Elements: A Spectral Approach*, Springer-Verlag, Berlin, 1991.
8. Gerristma, M., van der Steen, J. B., Vos, P., and Karniadakis, G. E., Stochastic computational fluid mechanics, *Comput. Sci. Eng.*, 9(2):21–29, 2007.
9. Rahman, S. and Yadav, V., Orthogonal polynomial expansions for solving random eigenvalue problems, *Int. J. Uncertainty Quantification*, 1(2):163–187, 2011.
10. Agarwal, N. and Aluru, N. R., A domain adaptive stochastic collocation approach for analysis of mems under uncertainties, *J. Comput. Phys.*, 228(20):7662–7688, 2009.
11. Xiu, D. and Karniadakis, G. E., The wiener-askey polynomial chaos for stochastic differential equations, *SIAM J. Sci. Comput.*, 24(2):619–644, 2002.
12. Rahman, S., Extended polynomial dimensional decomposition for arbitrary probability distributions, *J. Eng. Mech.*, 135(12):1439–1451, 2009.
13. Rahman, S., A polynomial dimensional decomposition for stochastic computing, *Int. J. Numer. Methods Eng.*, 76:2091–2116, 2008.
14. Gerristma, M., van der Steen, J. B., Vos, P., and Karniadakis, G. E., Time-dependent generalized polynomial chaos, *J. Comput. Phys.*, 229(2):8333–8363, 2010.
15. Wan, X. and Karniadakis, G. E., An adaptive multi-element generalized polynomial chaos method for stochastic differential equations, *J. Comput. Phys.*, 209(2):671–642, 2005.
16. Ma, X. and Zabaras, N., An adaptive hierarchical sparse grid collocation algorithm for the solution of stochastic differential equations, *J. Comput. Phys.*, 228(8):3084–3113, 2009.
17. Ma, X. and Zabaras, N., An adaptive high-dimensional stochasticmodel representation technique for the solution of stochastic pdes, *J. Comput. Phys.*, 229(10):3884–3915, 2010.
18. Soize, C., Maximum entropy principle for stochastic models in computational mechanics, *J. Thematique Incertitudes Groupement MoMaS*, Invited Lecture, Institut Henri Poincarè, Paris, 2008.
19. Ganapathysubramanian, B. and Zabaras, N., A seamless approach towards stochastic modeling: Sparse grid collocation and data driven input models, *Finite Elements Anal. Des.*, 44(5):298–320, 2008.
20. Klimke, A., Sparse grid interpolation toolbox userss guide, Stuttgart–Institut fur Angewandte Analysis und Numerische Simulation, 2008.
21. Sonmeza, H., Gokceoglua, C., Nefeslioglub, H., and Kayabasi, A., Estimation of rock modulus: For intact rocks with an artificial neural network and for rock masses with a new empirical equation, *Int. J. Rock Mech. Mining Sci.*, 43:224–235, 2009.
22. Soize, C., Construction of probability distributions in high dimension using the maximum entropy principle: Applications to stochastic processes, random fields and random matrices, *Int. J. Numer. Methods Eng.*, 76(10):1583–1611, 2008.

23. Sankaran, S. and Zabaras., N., A maximum entropy approach for property prediction of random microstructures, *Acta Mater.*, 54(8):2265–2276, 2006.
24. Jaynes, E., Information theory and statistical mechanics, *Phys. Rev.*, 106(4):1620–630, 1957.
25. Shannon, C. E., A mathematical theory of communication, *Bell Syst. Tech. J.*, 27:379–423 and 623–659, 1948.
26. Campillo, F., Parallel and interacting markov chain monte carlo algorithm, *Math. Comput. Simulation*, 79(12):3424–3433, 2009.
27. Tan, Z., Monte carlo integration with markov chain, *J. Stat. Planning Inference*, 138(7):1967–1980, 2008.
28. Carbonell, R., Desroches, J., and Detournay, E., A comparison between a semi-analytical and a numerical solution of a two-dimensional hydraulic fracture, *Int. J. Solids Struct.*, 36(31-32):4869–4888, 1999.
29. Rochinha, F. A. and Peirce, A., Monitoring hydraulic fractures: State estimation using an extended kalman filter, *Inverse Prob.*, 26(2):187–194, 2009.
30. Cornet, F., Doan, M., and Fontbonne, F., Eletrical imaging and hydraulic testing for a complete stress determination, *Int. J. Rock Mech. Mining Sci.*, 40:1225–1241, 2003.